Supporting Information

Highly Conductive and Flexible Ag NWs/PBFDO:PEOx Composite Transparent Electrodes Enabling Efficient Interfacial Tunneling Injection for OLED

Jiamin Sun [a], Guancheng Zhu [a], Zishuo Xu [a], Aoxue Yang [a], Feng Peng [c], Yangbing Huang [c], Haoran Tang [a], Jianhua Zou [b]*, Hong Tao [b], Lei Wang [a]*, Fei Huang [a], Junbiao Peng [a]*

E-mail: mstanghaoran@scut.edu.cn (H. Tang); zou1007@gmail.com (J. Zou); mslwang@scut.edu.cn (L. Wang)

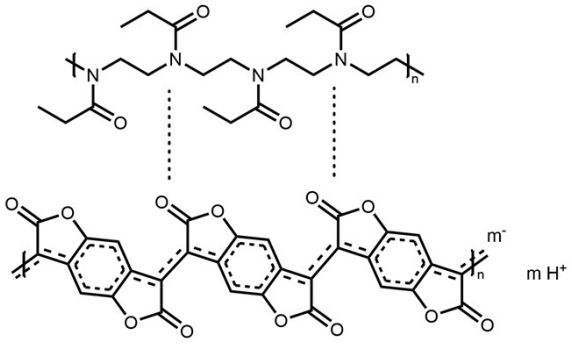

Figure S1. Chemical structure of PBFDO:PEOx.

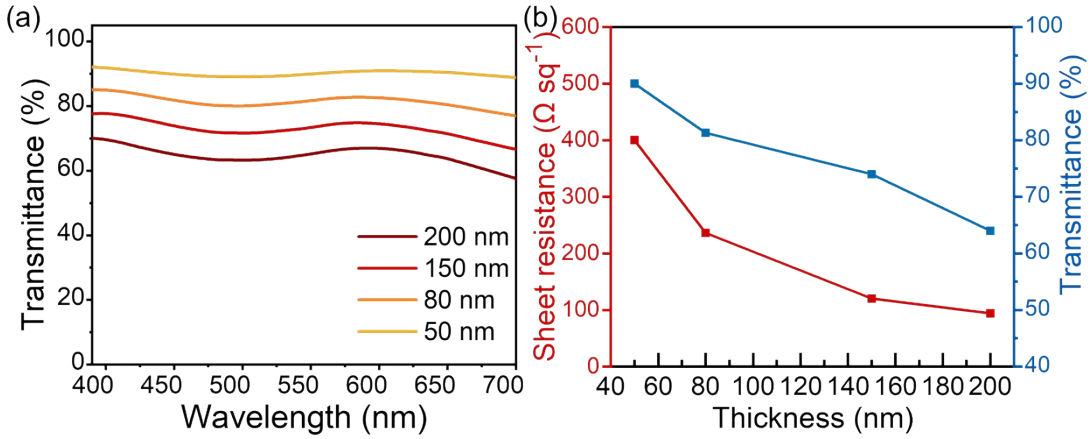

Figure S2. (a) Transmittance spectra of PBFDO:PEOx films with different thickness. (b) The dependence of sheet resistance and transmittance of PBFDO:PEOx films on film thickness.

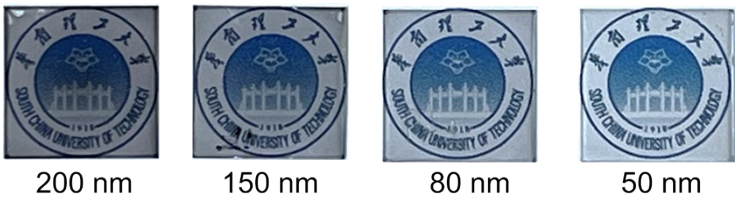

Figure S3. Photos of PBFDO:PEOx films with different thickness.

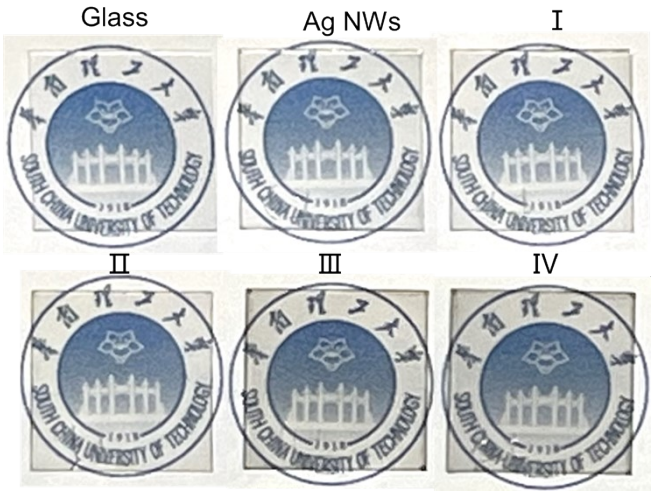

Fig S4. Photos of Ag NWs/PBFDO:PEOx composite films with different PBFDO:PEOx concentrations, pure Ag NWs film, and glass substrate.

Table.S1. Optoelectronic characteristics of different electrodes.

	Concentration of PBFDO:PEOx (mg/ml)	T_{550nm} (%)	R_s (Ω sq^{-1})	FoM
Film I	2.7	94	18	338
Film II	4.8	93	16	315
Film III	8	90	15	233
Film IV	12	86	12	199
PBFDO:PEOx	19.2	64	94	8
Ag NWs	-	95	65	113
ITO	-	94	12	507

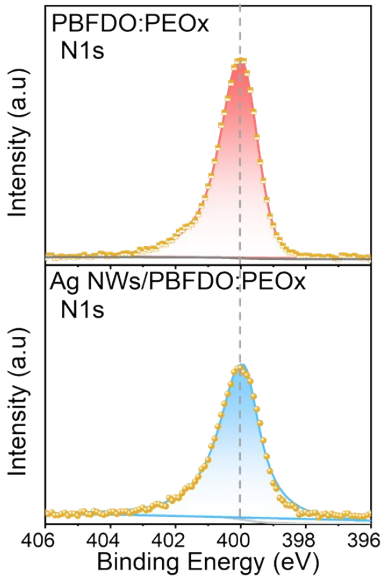

Figure S5. XPS spectra of N1s binding energy of PBFDO:PEOx and Ag NWs/PBFDO:PEOx

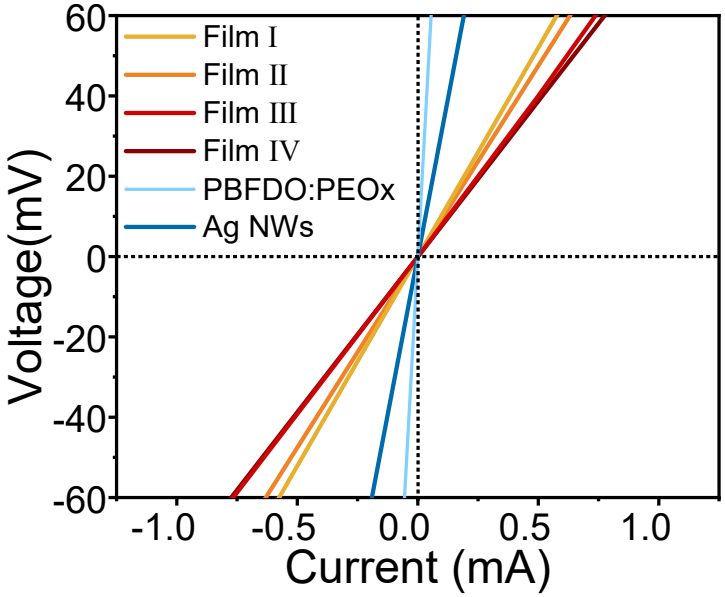

Figure S6. Current-voltage (*I-V*) curves of different films.

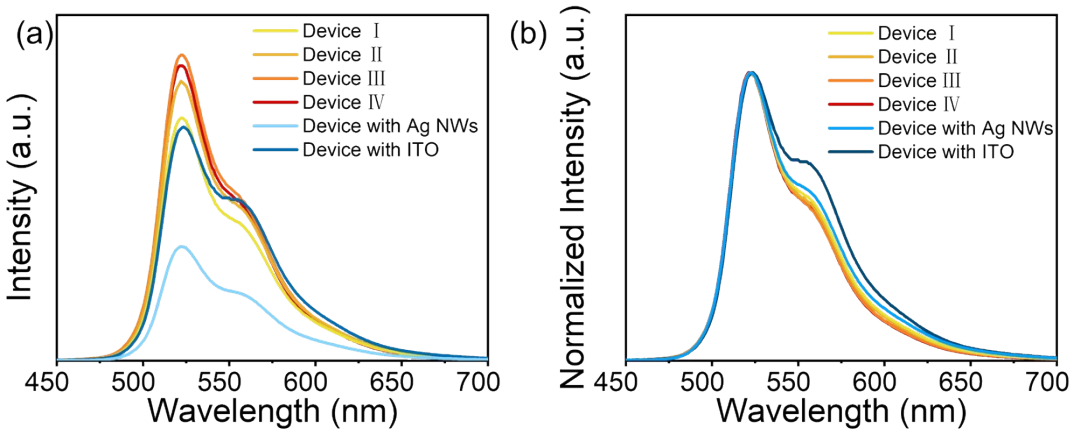

Figure S7. (a) EL spectra and (b) normalized EL spectra of devices with different electrodes.

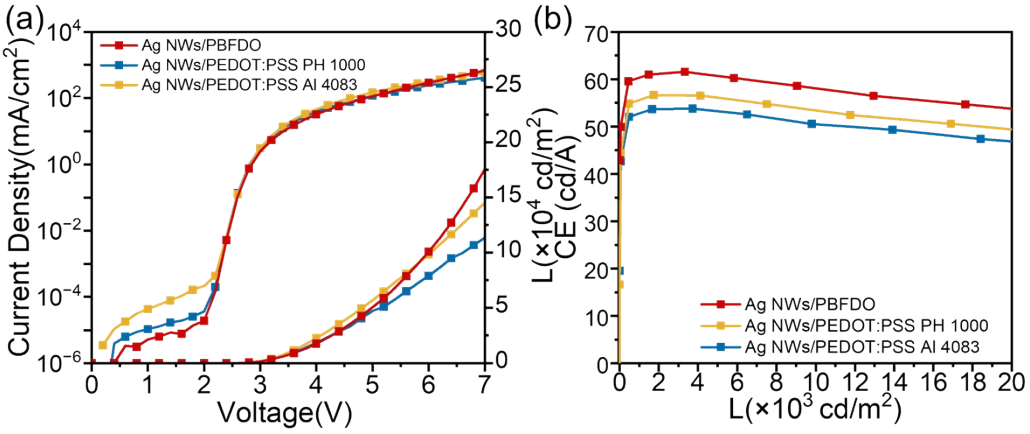

Figure S8. (a) *J*-*V*-*L*, and (b) CE-*L* characteristics of the OLEDs with different anodes.

Table S2. Performance OLEDs with different anodes.

	V_{on}	CE_{max}	At L = 1000 cd m^{-2}		
	(V)	(cd A^{-1})	V (V)	J (mA cm^{-2})	CE (cd A^{-1})
Device III	2.4	61.5	3	1.6	61.0
Device with PEDOT PH1000	2.4	56.6	3	1.7	57.9
Device with PEDOT AI 4083	2.4	53.8	3	1.9	53.0

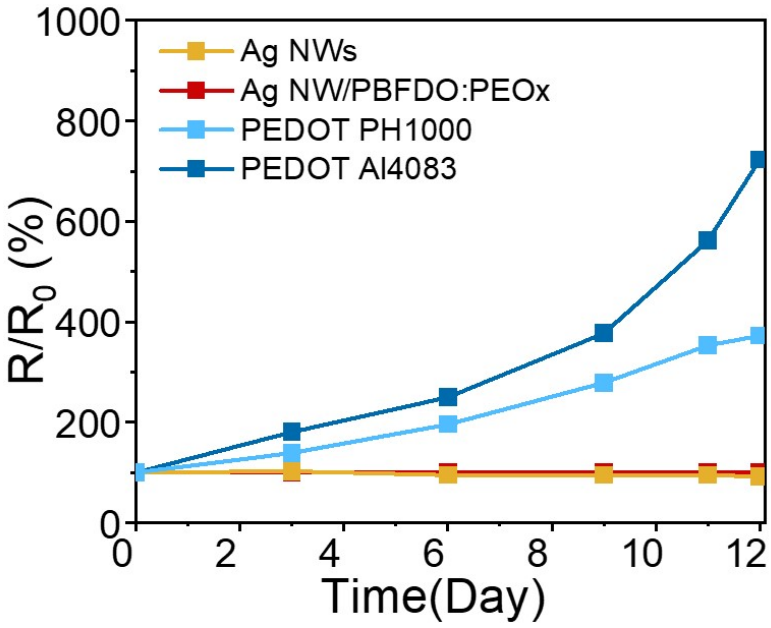

Figure S9. The electrical resistance changes of different electrodes after aging tests at 80°C.

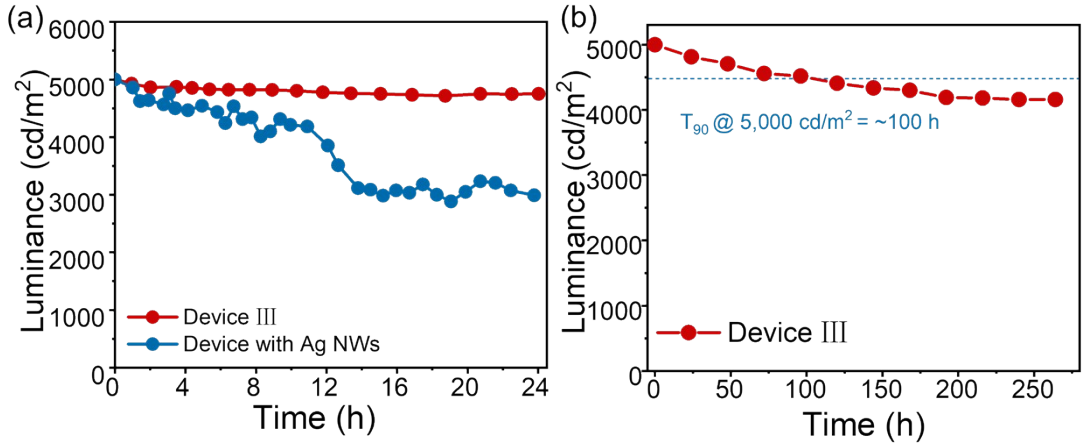

Figure S10. (a) Luminance-time curve of OLED devices based on pure Ag NWs electrode and Ag NWs/PBFDO:PEOx composite electrode under the initial luminance of 5000 cd/m^2. (b) Luminance-time curve of OLED devices based on Ag NWs/PBFDO:PEOx composite electrode under the initial luminance of 5000 cd/m^2.

Table.S3. Performance of flexible OLEDs with different electrodes.

	V_{on}	CE_{max}	At L = 1000 cd m^{-2}		
	(V)	(cd A^{-1})	V (V)	J (mA cm^{-2})	CE (cd A^{-1})
F-Device I	2.6	39.9	3.0	2.5	39.4
F-Device II	2.6	40.0	3.0	2.5	39.3
F-Device III	2.6	43.0	3.0	2.4	42.0
F-Device IV	2.6	37.6	3.4	2.7	36.6
F-Device with Ag NWs	2.6	19.5	3.6	6.2	16.1
F-Device with ITO	2.6	40.6	3.0	2.6	39.5

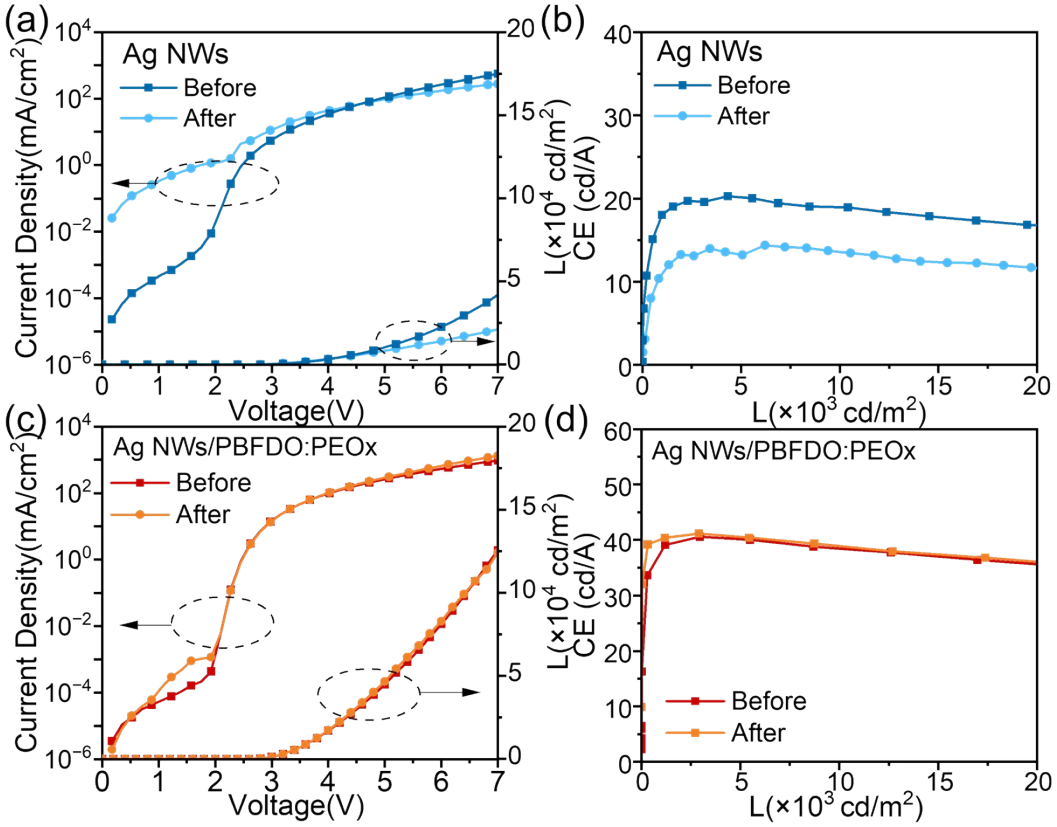

Figure S11. (a) The *J*-*V*-*L*, and (c) CE-*L* characteristics of the OLED devices with pure AgNWs anodes before and after bending. (c) *J*-*V*-*L*, and (d) CE-*L* characteristics of the OLED devices with AgNWs/PBFDO:PEOx anodes before and after bending.

Table S4. Performance OLEDs with different anodes before and after bending.

	V_{on}	CE_{max}	At L = 1000 cd m^{-2}		
	(V)	(cd A^{-1})	V (V)	J (mA cm^{-2})	CE (cd A^{-1})
Device with AgNWs-Before bending	2.4	20.6	3.4	5.6	18.0
Device with AgNWs-After bending	2.4	14.0	3.2	9.1	11.0
Device with AgNWs/PBFDO:PEOx-Before bending	2.4	40.6	3	2.6	39.1
Device with AgNWs/PBFDO:PEOx-After bending	2.4	41.1	3	2.5	40.4

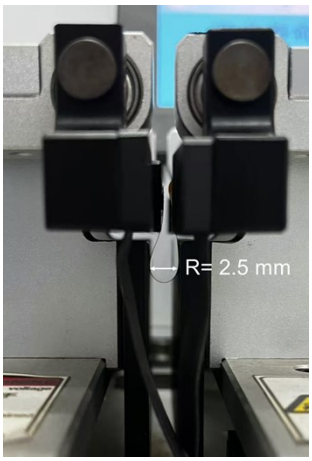

Figure S12. Image of the bending test machine and the bended film.